3D Flowerlike Micro/nanocomposite Ceria to Remove Arsenic and Chromium in Drinking Water

By

Taera Kim

* * * * * * * * *

Submitted in partial fulfillment

of the requirements for

Honors in the Department of Chemistry

UNION COLLEGE

June, 2014

ABSTRACT

KIM, TAERA 3D flowerlike micro/nanocomposite ceria to remove arsenic and chromium in drinking water. Department of Chemistry, June 2014.

ADVISORS: Laura A. MacManus-Spencer and Michael E. Hagerman

Ceria has received great attention for the removal of water contaminants due to its high oxygen storage capacity, marked oxygen ion conductivity, and tunable catalytic activity. Zhong *et al.* suggested that ceria (cerium oxide) microspheres with nanoscale 3D flowerlike morphology represent a promising inorganic synthetic material to remove water contaminants such as As(V) and Cr(VI) from drinking water. The 3D flowerlike micro/nanocomposite ceria offer key advantages over other nanoparticle based remediation systems as they can be easily removed via conventional microfiltration. The goals of this thesis project were to test the reproducibility of the synthesis of the 3D flowerlike ceria, and to assess the ability of the material to remove As(V) and Cr(VI) from water. Analyses using scanning electron microscopy (SEM), powder X-ray diffraction (XRD), and attenuated total reflectance-infrared spectroscopy (ATR-IR) confirmed the successful synthesis of the 3D flowerlike ceria. Inductively coupled plasma – mass spectrometry (ICP-MS) was used to quantify the removal of As(V) and Cr(VI) from water; results revealed that the concentrations of As(V) and Cr(VI) were reduced by more than 90% using the 3D flowerlike ceria, and their final concentrations were lower than the maximum contaminant levels set by the U.S. EPA. SEM images of both exposed and recycled 3D flowerlike ceria indicated that the 3D flowerlike morphology was retained after exposure to As(V) and Cr(VI) and after washing with NaOH solution. The 3D flowerlike ceria is an effective nanosorbent for the removal of As(V) and Cr(VI) in water treatment.

ACKNOWLEDGEMENTS

My thesis project was supported by the KANE Summer Research Fellowship, a Union College Presidential Green Grant, and the Union College Chemistry Department. I would like to give special thanks to my thesis co-advisors: Professor Laura A. MacManus-Spencer and Professor Michael E. Hagerman. Without their help and guidance, I would not have been able to undertake this project.

I would like to thank Professors Matthew Manon, James Adrian, and Joanne Kehlbeck for helping me with the experiments. I would also like to thank XiXi Hu, and my lab mates, Mike Morris, Erin Waterman, Isaac Ramphal, and Jared Mondschein. Lastly, I would like to extend my gratitude to faculty and staff members of the Union College Chemistry Department and the Schaffer Library.

TABLE OF CONTENTS

TABLE OF CONTENTS

TABLE OF FIGURES/TABLES

1. INTRODUCTION

Among the most serious environmental problems today is drinking water pollution caused by toxic substances like arsenic- and chromium-containing compounds, which are potential carcinogens and poisons.[1] More specifically, inhaled and ingested chromium(VI) can cause lung cancer and liver and kidney damage, respectively.[2] The maximum contaminant levels (MCLs) for arsenic(V) and chromium(VI) set by the U.S. Environmental Protection Agency (EPA) are 10 ppb[1] and 100 ppb,[3] respectively. Prior research has suggested that arsenic contamination in drinking water is a serious cause of poisoning in many countries, including Bangladesh.[4] According to the Washington Post, chromium contamination was found in the drinking water of 31 United States cities.[5] Although providing arsenic- and chromium-free water is urgent in places like Bangladesh and the United States, there are few effective and efficient water treatment methods to remove this contaminant.[4]

Nanomaterial science has received great attention for developing less expensive and more environmentally acceptable water purification methods including nanocatalysts, nanostructured catalytic membranes, nanoparticle enhanced filtration, and nanosorbents.[6] Nanoparticles are efficient water purification nanocatalysts and redox active media because of their large surface areas, size, and optical, electronic and catalytic properties, which are shape dependent.[7] Adesina has concluded that titanium dioxide (TiO_2) nanoparticles are very versatile because they can serve as oxidative and reductive catalysts, as well as photocatalysts for organic and inorganic pollutants in water purification processes.[8] Total organic carbon in contaminated water was greatly removed when TiO_2 nanoparticles were added in the presence of ultraviolet light.[8] Nanoscale zero valent iron (Fe_0) and biometallic Fe_p particles are paradigms of redox active media; these particles reduce organic and inorganic

pollutants in aqueous solutions to less toxic by-products.[9-11]

Nanostructured and reactive membranes, including nanofiltration and reverse osmosis, play an important role in purifying water. Vander Bruggen and Vandercasteele reviewed the effectiveness of nanofiltration to removal of cations, natural organic matter, biological contaminants, organic pollutants, nitrates and arsenic from groundwater and surface water.[12] Favre-Reguillon reported that nanofiltration is an effective method to remove minute quantities of uranium(VI) from seawater.[13] Peltier et al. concluded that water quality for a large water distribution system improved using nanofiltration, reducing organic and biological contaminants.[14]

However, both nanofiltration and reverse osmosis methods require a pressure gradient to selectively transport solvent and certain solutes across a membrane.[1] Nanofiltration requires a pressure gradient of 345 to 1034 kPa (50 to 150 psi), whereas reverse osmosis requires a pressure gradient of 689 to 1034 kPa (100 to 150 psi).[1] In addition to nanofiltration and reverse osmosis, the invention of dendritic polymers in the area of macromolecular chemistry made a significant contribution to the development of ultrafiltration processes for water purification. Dendritic polymers, which are soft nanoparticles with the size of 1-20 nm, can be used as recyclable water-soluble ligands with high capacity for toxic metal ions, radionuclides, and inorganic anions.[15-17]

Nanosorbents are widely used to remove organic and inorganic pollutants from contaminated water due to their large surface areas and functionality with chemical groups to have high affinity towards target compounds.[6] Li *et al*. have investigated the sorption capacities of multiwalled carbon nanotubes (MWCNTs) for lead(II), copper(II), and cadmium(II).[18] They reported that the metal-ion sorption

capacities of the MWCNTs were 3 to 4 times greater than those of powder activated carbon and granular activated carbon, which are the two common sorbents used in water purification.[18] Moreno *et al*. have evaluated NaP1 zeolites ($Na_6Al_6Si_{10}O_{32} \cdot 12H_2O$) as effective sorbents and ion-exchange media for the removal of heavy metal ions from acid mine wastewaters.[19]

Peng *et al*. have incorporated cerium oxide, which is also known as ceria and has high surface area (189 m^2/g), on carbon nanotubes (CeO_2-CNTs), and these particles appeared to be effective nanosorbents for arsenic(V).[20] The addition of calcium(II) and magnesium(II) increased the amount of sorbed arsenic(V) approximately from 10 to 82 mg/g.[19] In addition to CeO_2-CNTs, Deliyanni *et al*. have developed akaganeite [b-FeO(OH)] nanocrystals for a novel arsenic(V) sorbent.[21] Lazaridis *et al*. reported that nanocrystalline akaganeite is also an effective chromium(VI) sorbent.[22]

In contrast to these nanomaterials, Zhong *et al*. successfully synthesized 3D flowerlike ceria and confirmed that 3D flowerlike ceria is an effective nanosorbent for the removal of both arsenic(V) and chromium (VI).[23] 3D flowerlike ceria can be synthesized in a manageable and economical way to remove arsenic and chromium pollutants, and it can be reused many times.[23] People not only in Bangladesh and in the United States, but also in other countries where water contamination is a serious problem, may benefit from using 3D flowerlike ceria.

1.1 System of Interest

1.1.1 Ceria

Ceria is a synthetic inorganic compound which has a high oxygen storage capacity because it can shift from CeO_2 to Ce_2O_3.[24] Bulk ceria can remove

contaminants through catalytic reactions such as the reduction of NO to N_2,[25] the oxidation of CO and unburned hydrocarbons,[22] and the conversion of SO_2 to H_2S,[25] and through adsorption such as the adsorption and release of H_2S from gas streams.[26] Nanoscale ceria is more efficient for catalysis and adsorption because of its higher surface area and increased catalytic activity compared to that of bulk ceria.[23] It has previously been shown that ceria nanoparticles supported on carbon nanotubes adsorb significant amounts of both arsenic[27] and chromium[28] from contaminated water.

However, nanoparticles are difficult to recover for recycling because they are too small to be removed via conventional microfiltration.[29] Hence, it is important to synthesize ceria microspheres with nanoscale features. The micro/nanocomposite structure maintains nanoscale properties such as surface area and makes the composite more facile to handle. The 3D flowerlike micro/nanocomposite ceria is superior to other water purification methods due to the following reasons: (i) the possibility of separation and recycling, (ii) high surface area, and (iii) prevention of aggregation, retaining unblocked mass transfer and high catalytic activity.[23] Most importantly, ceria may be reused multiple times by washing in sodium hydroxide solution to remove sorbed contaminants[23] and does not require a pressure gradient or the discharge of a great amount of water as with nanofiltration and reverse osmosis.

1.1.2 Proposed Mechanism for Formation of Ceria

One proposed mechanism for ceria formation is outlined in Scheme 1.[30] A portion of the ethylene glycol becomes oxidized as it reacts with molecular oxygen during reflux to form oxalic acid and formic acid. Formate and oxalate bind to the cerium(III) cations present to form the ceria precursor which contains alkoxide bridging ligands. Lastly, cerium formate complexes with oxalic acid, which is the

bridging unit, to form cerium alkoxide nanomaterials with spindle structures. Each cerium formate unit in the cerium alkoxide chain has an octahedral geometry that is stabilized by formic acid.

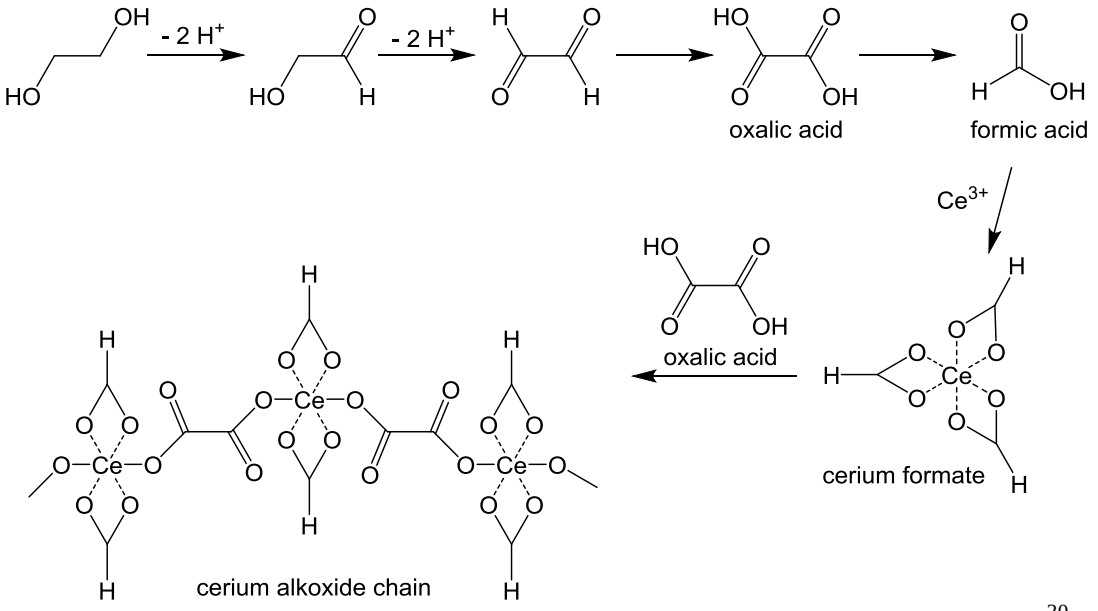

Scheme 1. Proposed mechanism for the formation of spindle ceria nanomaterials.[30]

Sun *et al.* reported a proposed mechanism for monodispersed flowerlike ceria microspheres (Scheme 2).[31] The flowerlike ceria microspheres were synthesized mainly by a polymerization-precipitation reaction, metalmorphic reconstruction, mineralization, and controlled calcinations.[31] Sun *et al.* suggested that this mechanism can be used to synthesized other 3D flowerlike nanostructures owing to the morphological preservation of both individual ceria nanosheets and 3D flowerlike microspheres upon calcination.[31] However, there are few studies on 3D flowerlike micro/nanocomposite structure of ceria. Perhaps the most likely proposed mechanism for formation of 3D flowerlike micro/nanocomposite ceria is a combination of Schemes 1 and 2 because ethylene glycol is used to form a cerium alkoxide chain and then ultimately 3D flowerlike micro/nanocomposite ceria.

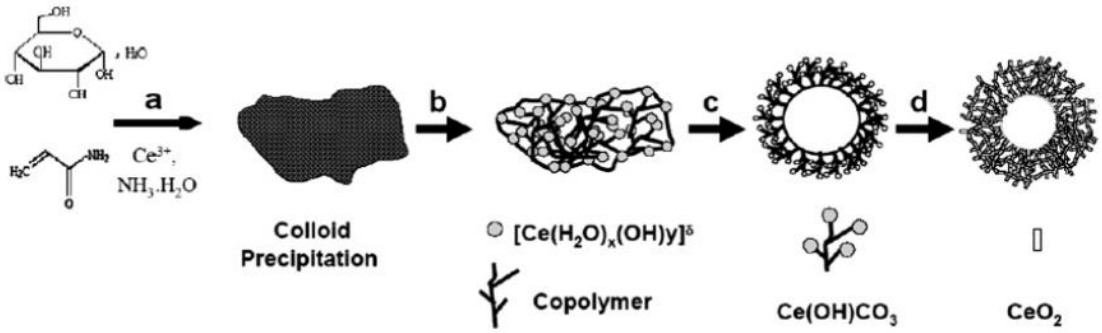

Scheme 2. Proposed mechanism for formation of flowerlike ceria microspheres.[31]

1.1.3 Laponite and Ceria/Laponite Water Filtration Membrane

Laponite is synthetic hectorite clay which consists of disc-shaped nanoparticles that are approximately 25 nm in diameter and 0.92 nm in thickness and has a negative surface charge density of 0.014 $e^{-}/Å^{2}$ in water.[32] An isotropic liquid phase, a gel phase, and a nematic gel can be formed at low salt concentration and increasing clay weight.[33-34] It can be used to coat various substrates through facile self-assembly from the aqueous phase. Its self-assembly is significant because it facilitates the fabrication of organic-inorganic nanocomposites.[35] Nanoparticles can be used to form Laponite membranes through the self-assembly of Laponite such as nano-Laponite/CdSe and Laponite/Polyaniline.[36] More importantly, a Laponite/ZnO membrane was created to remove trichloroethylene (TCE), a common water contaminant.[37] Similar to the Laponite/nano-ZnO membrane, 3D flowerlike ceria may be included to form a Laponite/ceria membrane, which will ideally sequester toxic metals such as arsenic and chromium while allowing water to pass through the membrane.

In this study, the formation of 3D flowerlike ceria is studied using Powder X-ray Diffraction (XRD) and Scanning Electron Microscopy (SEM). The chemical composition of ceria is analyzed using attenuated total reflectance infrared

spectroscopy (ATR-IR). The ability of ceria particles to remove arsenic(V) and chromium(VI) contaminants is tested using inductively coupled plasma-mass spectrometry (ICP-MS).

1.2 Characterization Methods

1.2.1 ATR-IR

Infrared spectroscopy (IR) is used to measure the absorption of IR radiation by a molecule by exciting a molecule from a ground energy state to a higher vibrational energy state. Absorption occurs when the frequency of stretching and bending of the specific bonds in a molecule matches the frequency of the incident radiation.[38] In order for molecules to absorb IR radiation, there must be a vibrational motion that causes a change in dipole moment.[38] The common modes of vibration are stretching vibrations (symmetrical and asymmetrical) and bending vibrations. A symmetrical stretching vibration of a symmetrical molecule is called IR-inactive because it does not change the dipole moment of the molecule.[38] On the other hand, a symmetrical stretching of an asymmetrical molecule, asymmetrical stretching vibrations and bending vibrations are IR-active because they cause changes in the dipole moment of the molecule. The frequency at which IR radiation is absorbed depends on several factors such as the masses of the atoms in the bond, the strength of the bond, and the geometry of the molecule.[38]

For an IR radiation source, the intensity of radiation should be continuous over the wavelength range, be constant over time, and should cover a broad wavelength range.[38] One of the most common modern sources for the mid-IR radiation is the Globar, which is an electrically heated bar of sintered silicon carbide.[38] The sample holder in an IR spectrometer must be transparent to IR radiation in order

to observe the absorption of the sample. Thus, materials such as glass or quartz cannot be used because these materials absorb IR radiation at wavelengths longer than 3.5 μm.[38]

One common IR sampling techniques is ATR-IR, which can be used for the analysis of films, solids, and liquids. A small quantity of liquid or solid sample is placed in contact with the surface of the internal reflection element (IRE). When the incoming light penetrates the sample, the light reflected becomes attenuated at certain frequencies where the sample absorbs.[38] A diagram of ATR-IR instrumentation is shown in Figure 1.

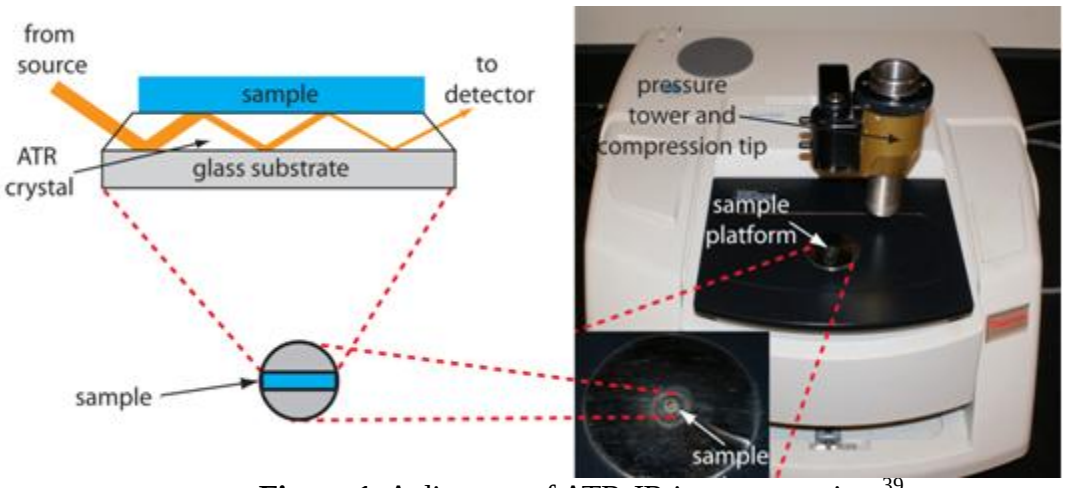

Figure 1. A diagram of ATR-IR instrumentation.[39]

The radiation emitted by the Globar is polychromatic. After the radiation passes through the sample, an interferometer collects all the wavelengths at the same time without dispersion.[38] The beam splitter splits the radiation coming from the source into two beams of equal intensity, after which the two beams are reflected back to the detector by a moving mirror and a fixed mirror.[40] By altering the position of the moving mirror, an interferogram is created, which is a time domain signal. Then, a Fourier transform is used to convert the signal to the frequency domain. ATR-IR requires a fast detector such as a pyroelectric detector.[38] In this study, ATR-IR was

used to analyze the chemical composition of the ceria precursor and the calcined ceria.

1.2.2 SEM

SEM is an electron microscope that focuses a high-energy electron beam onto the sample surface to generate images on the micro- to nanoscale;[41] this technique can also provide information about surface morphology and chemical composition, depending on the detection method used. The essential components of SEM include the following: an electron gun, electron lenses, a sample stage, a secondary electron detector or additional detectors, including a backscattered electron detector (BSE), an energy dispersive X-ray detector (EDX), or a cathodoluminescence detector (CL).[42] An electron gun is a tungsten filament that is wreathed with a Wehnelt electrode.[43] The negative potential of the Wehnelt electrode is what makes the electron gun a point source because electrons are emitted from a small area of the filament.[43] It is crucial to have a point source because a point source emits electrons that have the same kinetic energy; thus, using a point source ensures that any difference in signals results from the surface of the sample, not from the source of electrons.[44] As the electron beam passes through the scan coils and the deflecting objective lens, the focused beam of electrons rasters (*i.e.*, sweeps) over the surface of the sample. As a result, secondary electrons are produced due to the interactions between the incident electron beam and weakly bound conduction band electrons in the sample from a depth of 0.5 to 50 nm.[45] A secondary electron detector detects the secondary electrons that are accelerated by the high voltage applied to the tip of the secondary electron detector and produces images in a very fine scale.[44] SEM is conducted to study the surface morphologies of 3D flowerlike ceria particles. A diagram of SEM instrumentation is shown in Figure 2.

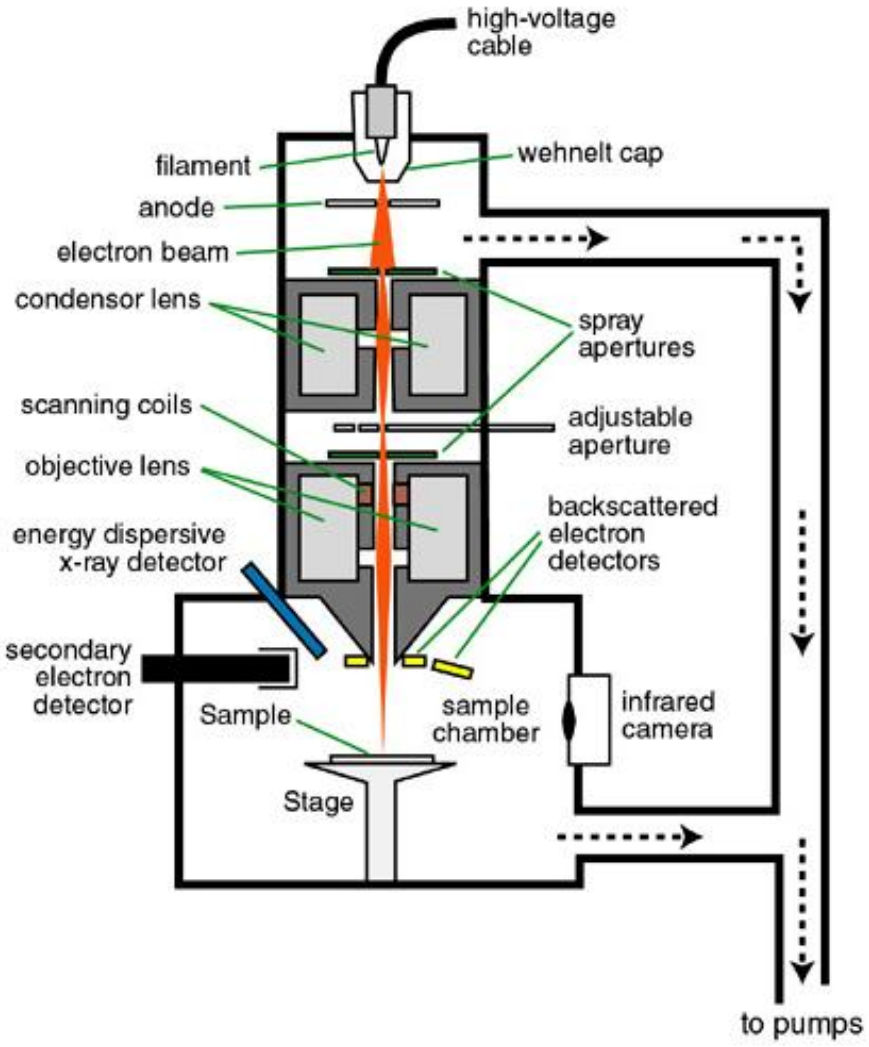

Figure 2. A diagram of SEM instrumentation.[42]

1.2.3 Powder XRD

Powder XRD is a technique that is used to determine the atomic and molecular structure of solid crystalline or semicrystalline materials.[41] X-ray diffraction occurs when the incident beam of X-rays is reflected by the atomic planes of a crystal, and the reflected beam interacts with other reflected beams, reinforcing each other.[38,41] The distance between the planes of electron density in crystals can be measured using the Bragg equation (Equation 1, Figure 3)

$$n\,\lambda = 2\,d\,\sin\theta \qquad (1)$$

where *n* is the order of diffraction, λ is the known wavelength of the monochromatic X-ray beam, *d* is the distance between planes of electron density in the crystal, and θ the angle between the incident X-ray beam and the surface of the crystal.

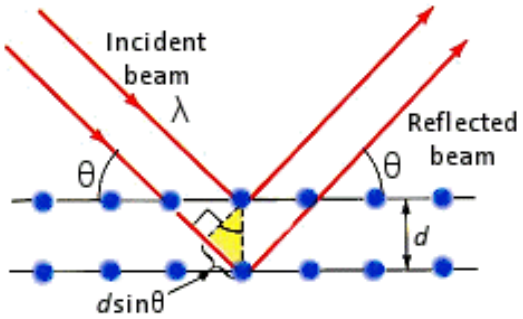

Figure 3. A schematic diagram of Bragg's equation.[46]

The measurement of the distance between planes of electron density in crystals determines the crystal structure of solid crystalline or semicrystalline materials.[38] Non-crystalline materials such as liquids, gases, and solids, including glasses and amorphous polymers, cannot be studied by XRD; these materials do not show the diffraction of X-rays because they do not have a well-ordered structure. In powder XRD, the diffraction pattern is obtained from a powder of the material, not an individual crystal. The advantages of using powder XRD are the following: no single crystals are needed, peaks can be seen due to various elements, and speciation (*i.e.*, oxidation states) can be analyzed.[46]

For XRD sample preparation, materials must be ground and pressed to form a flat surface in the sample holder. A powdered sample emits the circular cones of diffracted X-rays due to the random orientation of crystallites in the sample. The circular cones of X-rays result in curved lines on the X-ray film as the X-ray film is curved to fit the diameter of the Rowland circle.[38] The sample rotates relative to the X-ray source, which remains stationary, at a rate of θ/min.[38] A charge coupled device (CCD), which is a two-dimensional array detector, simultaneously rotates at a rate of

2θ/min along the sample and detects diffracted radiation released by the sample according to the Bragg equation.[38] XRD is used to get information about the elements of 3D flowerlike ceria particles and oxidation states present.

1.2.4 ICP-MS

ICP-MS is a type of mass spectrometry that can be used to detect and quantify metals and non-metals at very low concentrations, such as parts per billion (ppb) and parts per trillion (ppt), typically with unit mass resolution.[38] This technique has great advantages over other techniques for quantitative elemental analyses because it has a high scan rate, high sensitivity, high selectivity, and good precision and accuracy.[37] It has applications in environmental chemistry such as analyses of water, wastewater, soil, sediment, and air particulates.[38]

The sample preparation for water samples is relatively simple. Samples are acidified with 1% nitric acid. Nitric acid has advantages over other strong acids because it causes the least amount of polyatomic ion interferences except for one silicon isotope (^{28}Si).[47] The concentration of solutions is kept less than 1000 parts per million (ppm), preferably less than 500 ppm.[48] Standards are prepared which have similar concentrations as the analytes. Internal standards that have masses similar to the analyte metals are also prepared to correct some aspects of instrumental drift. The common internal standards for water samples are beryllium (Be), strontium (Sr), gallium (Ga), yttrium (Y), indium (In), praseodymium (Pr), rhenium (Re), bismuth (Bi), and thorium (Th).[47] Glassware cannot be used to prepare and contain the metal solutions because metals tend to interact with and adhere to glass. Thus, plastic volumetric flasks and tubes are used for all sample preparation procedures.

The typical ionization source in ICP-MS is an argon plasma. An argon ionization source gives high ionization efficiency because it has an ionization energy of 15.8 eV, which is higher than that of all elements on the periodic table except for helium (He), neon (Ne), and fluorine (F).[40] An excited argon (Ar) atom collides with analyte elements to produce ions in an Ar plasma, which has a temperature of 6,000 – 10,000 K.[49] It produces mostly monoatomic ions with a single positive charge[38] and small diatomic species.[49] The resulting ions enter a quadrupole mass analyzer, which separates ions based on their mass-to-charge ratio (m/z) in an electric field.[38] This electric field is created when an oscillating radio frequency voltage and a constant direct current voltage are applied to four parallel metal rods. At a given radio frequency to direct current voltage ratio, only ions of the correct mass-to-charge ratio take a corkscrew-like path through the quadrupole and reach the electron multiplier detector, whereas other ions that have unstable trajectories collide with the rods. An electron multiplier detector detects analyte ions that pass through the quadrupole mass analyzer, producing a cascade of electrons for each ion.[38] Signals are proportional to the concentration of analyte ions. A diagram of ICP-MS instrumentation is shown in Figure 4.

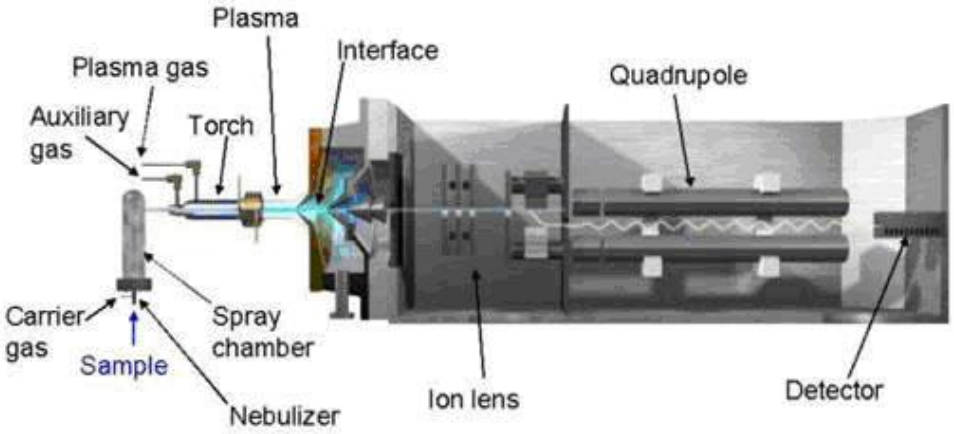

Figure 4. A diagram of ICP-MS instrumentation.[50]

It is important to note that isobaric interference, one of the mass spectral interferences, occurs when there are ionic species present in the plasma that have the same m/z values as the analyte ion of interest. Since many Ar^+ ions are present in the plasma, the ions of Ar, such as ArH^+, ArC^+, ArN^+, $ArNH^+$, ArO^+, $ArCl^+$, and Ar_2^+, interfere with analyte ions that have the same m/z.[40] Isobaric interference often occurs with the most abundant isotope because the most abundant isotope is the most sensitive.[51] For instance, $^{40}Ar^+$ interferes with the most abundant calcium isotope $^{40}Ca^+$ (97%); thus, the second-most abundant calcium isotope $^{40}Ca^+$ (2.1%) must be analyzed.[51] In addition, ArC^+ interferes with $^{52}Cr^{6+}$, so the isotope ^{53}Cr should be analyzed. Here, ICP-MS was used to measure arsenic(V) and chromium(VI) concentrations in contaminated and purified water samples to test the removal efficiencies of 3D flowerlike ceria particles and films.

1.3. Research Goals

The main goals of this research are the following: 1) to synthesize ceria micro/nanocomposite structures for water filtration studies, 2) to test their ability to

remove As(V) and Cr(VI) from water, 3) to fabricate Laponite/ceria membranes, and 4) to learn the synthesis and characterization of nanomaterials that have interdisciplinary applications in environmental science.[52]

2. EXPERIMENTAL

2.1 Materials

Anhydrous cerium chloride (>99.99%), cerium chloride heptahydrate ($CeCl_3 \cdot 7H_2O$, 99.999%), urea, tetrabutylammonium bromide (98.8%), ethylene glycol (99.8%), ethanol (99.5%), sodium arsenate dibasic heptahydrate (98.0%), and potassium dichromate (99.0%) were purchased from Sigma-Aldrich and were used without further purification. Hydrochloric acid and sodium hydroxide were purchased from Fisher Scientific. The high-purity 70% nitric acid was distilled in a two-bottle Teflon still by staff in the Union College Geology department. ^{69}Ga, ^{59}Pr, and ^{45}Sc were purchased from Inorganic Ventures. Laponite RD was purchased from Southern Clay Products.

2.2 Synthesis of Ceria

Anhydrous $CeCl_3$ (0.7548 g), urea (1.1039 g), and TBAB (0.2996 g) were added to 75 mL ethylene glycol in a 250-mL three-necked round bottom flask. The mixture was stirred with a magnetic stir bar and was heated using a heating mantle at 180℃ for 30 min. The solution was cooled down to room temperature when the reaction was complete. The precipitate was washed with ethanol four times in a 50-mL PPCO copolymer centrifuge tube for 30 min at 1684 rcf (4000 rpm, r_{max} = 94.0 mm) in an Allegra X-22R Centrifuge and was dried in air for a day. The air-dried precipitate was calcined at 450℃ for 24 h and was cooled down to room temperature

for a day.

After failure to obtain 3D flowerlike ceria, $CeCl_3 \cdot 7H_2O$ was used as a cerium source instead of anhydrous $CeCl_3$. $CeCl_3 \cdot 7H_2O$ (1.5015 g), urea (2.2008 g), and TBAB (6.0005 g) were added to 150 mL ethylene glycol in a 250-mL round bottom flask. The mixture was stirred with a magnetic stir bar and was heated at 180℃ in an oil bath for 30 min in this experiment. The solution was cooled down to room temperature when the reaction was complete. The precipitate was washed with ethanol four times in a 50-mL PPCO copolymer centrifuge tube for 30 min at 1684 rcf (4000 rpm, r_{max} = 94.0 mm) in an Allegra X-22R Centrifuge and was dried in air for a day. A small amount of the air-dried precipitate was collected as the ceria precursor. The rest of the air-dried precipitate was calcined at 450℃ for 24 h and was cooled down to room temperature for a day; this final product was collected as the calcined ceria.

2.3 Removal of As(V) and Cr(VI) from Water

As(V) and Cr(VI) solutions were prepared using $Na_2AsO_4 \cdot 7H_2O$ and $K_2Cr_2O_7$ as the sources of As(V) and Cr(VI). The $Na_2AsO_4 \cdot 7H_2O$ (0.0259 g) and $K_2Cr_2O_7$ (0.0259 g) were added to separate 10-mL polypropylene volumetric flasks and diluted with deionized water, which resulted in concentrations of 621.9 ppm and 915.5 ppm of As(V) and Cr(VI), respectively. For 1:100 dilutions, 100 µL of 621.9 ppm As(V) solution and 915.5 ppm Cr(VI) solution were added to 10-mL polypropylene volumetric flasks and diluted with deionized water. To have final concentrations of 80 ppb for both As(V) and Cr(VI) solutions, 128.6 µL of 6.219 ppm As(V) solution and 87.4 µL of 9.155 ppm Cr(VI) solution were added to 10-mL polypropylene volumetric flasks in triplicate (*i.e.*, three controls and three test samples

both for As(V) and Cr(VI) solutions) and diluted with deionized water. In addition, 128.6 µL of 6.219 ppm As(V) solution and 87.4 µL of 9.155 ppm Cr(VI) were added together to 10-mL polypropylene volumetric flasks in triplicate (*i.e.*, three controls and three test samples) and diluted with deionized water for the mixed As(V) and Cr(VI) solutions. The pH of the 80 ppb As(V) and Cr(VI) solutions was adjusted to 3 by adding HCl or NaOH.

Then, 20 mg of the calcined ceria was added to three test samples in 15-mL ICP-MS polypropylene conical tubes for As(V), Cr(VI), and the mixed As(V) and Cr(VI) solutions, and these solutions were mixed on an orbital shaker table for 5 h at 100 rpm at room temperature. Controls for As(V), Cr(VI), and the mixed As(V) and Cr(VI) solutions were carried through the entire procedure except for the addition of 20 mg of the calcined ceria. Then, the exposed ceria was washed with 30 mL of 0.2 M NaOH on the orbital shaker table for 5 h at 100 rpm and was centrifuged for 2 h at 10,000 rpm. The supernatant was removed, and the recovered ceria was air-dried. The centrifuge tube containing ceria that was exposed to the As(V) solution broke, so only ceria that was exposed to Cr(VI) and the mixed As(V) and Cr(VI) solutions was recovered.

2.4 SEM

A Zeiss EVO50XVP instrument was utilized for SEM studies. Ceria precursor, the calcined ceria, ceria that was exposed to the mixed As(V) and Cr(VI) solution, and the recovered ceria that was exposed to the mixed As(V) and Cr(VI) solutions and was also washed in NaOH solution were mounted on SEM stubs with carbon tape. SEM images of these samples were obtained with the optimized accelerating voltage within a range from 8 to 20 keV and the optimized spot size

within a range from 259 to 429. A secondary electron detector was used to acquire the images.

2.5 ATR-IR

A Galaxy 6020 Fourier-Transform Infrared Spectrophotometer was used for ATR-IR studies. Small quantities of TBAB, ceria precursor, and the calcined ceria were placed on the IRE, and infrared spectra of these samples were obtained with 32 scans and 2 cm^{-1} resolution.

2.6 Powder XRD

A Phillips Compact X-ray Diffractometer System (PW1840) was used for powder XRD studies, which was operated at a voltage of 45 keV and a current of 35 mA. Iron filtered cobalt radiation was used with a wavelength of 1.790 Å. All XRD spectra were obtained using a step size of 0.010° (2θ) at 2.00 s per step and a receiving slit of 0.3 mm.

2.7 ICP-MS

2.7.1 Instrumentation

A PerkinElmer/Sciex Elan 6100 DRC was utilized for ICP-MS studies. Prior to the experiment, an Ar plasma was generated at 6000 ℃ for at least 30 min. The pressure of the vacuum system was 1.11×10^{-5} torr for the ion optics, quadrupole and detector.

2.7.2 Preparation of Blank, Working Standard, and Internal Standard Solutions

A blank solution was prepared by adding 7 mL of 70% nitric acid (HNO_3) to

a 50-mL polypropylene volumetric flask and diluting to 50 mL with high-purity deionized water using a Barnstead Easypure II purifier. To prepare working standard solutions, 0.5 mL of each 1000 ppm As and Cr stock solution and 7 mL of 70% HNO_3 were added and diluted to 100 mL, which resulted in a concentration for each of 5000 ppb. Then, 0.01 mL, 0.1 mL, 0.5 mL, and 1.0 mL of 5000 ppb As and Cr solutions were added and diluted to 50 mL with high-purity deionized water to make standards of 1 ppb, 10 ppb, 50 ppb, and 100 ppb with 1% HNO_3, respectively. The internal standards were the following: ^{69}Ga, ^{59}Pr, and ^{45}Sc. For a trace element internal standard solution, 0.1 mL of each 1000 ppm Ga, Sc, and Pr stock solution and 7 mL HNO_3 were added and diluted to 100 mL with high-purity deionized water. Then, 0.5 mL of internal standard solution was added to the blank and all working standard solutions. Lastly, 0.1 mL of internal standard solution, and 0.14 mL of 70% HNO_3 were added to all test solutions in 10-mL centrifuge tubes. In order to measure the concentrations of As(V) and Cr(VI) in the prepared solutions, $^{75}As(V)$ and $^{52}Cr(VI)$ were analyzed, as well as the isotope $^{53}Cr(VI)$ because ArC^+ interferes with $^{52}Cr(VI)$.

2.7.3 Analyses of As(V), Cr(VI), and the Mixed As(V) and Cr(VI) Solutions

A blank solution, four standard solutions, and the following solutions in triplicate were analyzed: As(V) controls, As(V) test samples, Cr(VI) controls, Cr(VI) test samples, the mixed As(V) and Cr(VI) controls, and the mixed As(V) and Cr(VI) test samples.

2.8 Investigation of the Dispersion of Laponite RD in the As(V) and Cr(VI) Solutions

The quantities of Laponite RD described in Table 1 were added to 80 ppb As(V) and 80 ppb Cr(VI) solutions in 15-mL polypropylene conical tubes, and these

solutions were mixed on an orbital shaker table for 5 h at 100 rpm at room temperature. Then, these solutions were centrifuged in 50-mL PPCO copolymer centrifuge tubes for 2 h at 0 ℃ and 10528 rcf (10000 rpm, r_{max} = 94.0 mm) in an Allegra X-22R Centrifuge.

Table 1. The quantities of Laponite RD added to 80 ppb As(V) and 80 ppb Cr(VI) solutions in triplicate without ceria.

Experiment	Amount of Laponite RD (mg)
1	75
2	50
3	25
4	10

3. RESULTS AND DISCUSSION

3.1 Characterization of 3D Flowerlike Ceria

3.1.1 SEM

SEM images revealed the morphological changes between the nanocomposite ceria (Figure 5) and the 3D flowerlike ceria (Figure 6). As shown in Figure 5, nanocomposite ceria was formed when anhydrous $CeCl_3$ was used as a reactant for the metal source. Many ceria nanomaterials appeared to clump together (Figure 5), and some of them were in a shape of nanowires (Figure 5). Since 3D flowerlike ceria did not form when using anhydrous $CeCl_3$ as a source of cerium and a heat mantle for the reflux setup, $CeCl_3 \cdot 7H_2O$ was used as the source of cerium and an oil bath with temperature control were utilized for the reflux setup to maintain the temperature at 180 ℃.

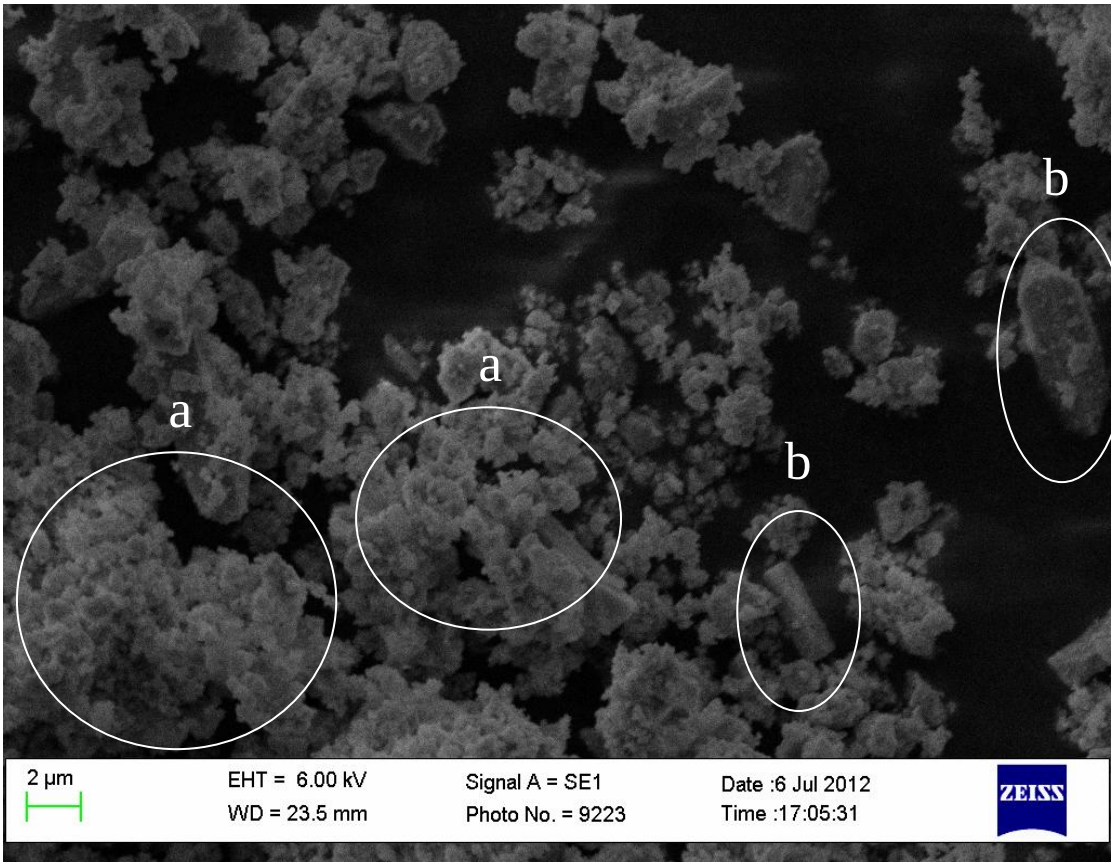

Figure 5. Formation of nanocomposite ceria when the synthesis of ceria was carried out at 180 ℃ using anhydrous cerium chloride as the source of cerium: (a) the ceria aggregates and (b) the ceria nanowires.

Shown in Figure 6, 3D flowerlike ceria successfully formed using the new parameters. Hence, it is crucial to utilize cerium chloride hydrate and a temperature-controlled oil bath for the synthesis of 3D flowerlike ceria. The water molecules of $CeCl_3 \cdot 7H_2O$ may stabilize the central Ce^{3+} ion and increase its solubility in ethylene glycol. The increased solubility of $CeCl_3 \cdot 7H_2O$ in ethylene glycol may facilitate the reaction between $CeCl_3 \cdot 7H_2O$ and formic acid to form cerium formate (Scheme 1). It is also possible that the water molecules of $CeCl_3 \cdot 7H_2O$ may form hydroxide ions. These hydroxide ions may interact and form Ce-O bonds which are the bridges of the ceria. In addition, the calcined ceria shown in Figure 6 shows evidence of micropetals that are composed of many compact layers. These stacked lamellae have been reported previously by Zhong *et al.*[23]

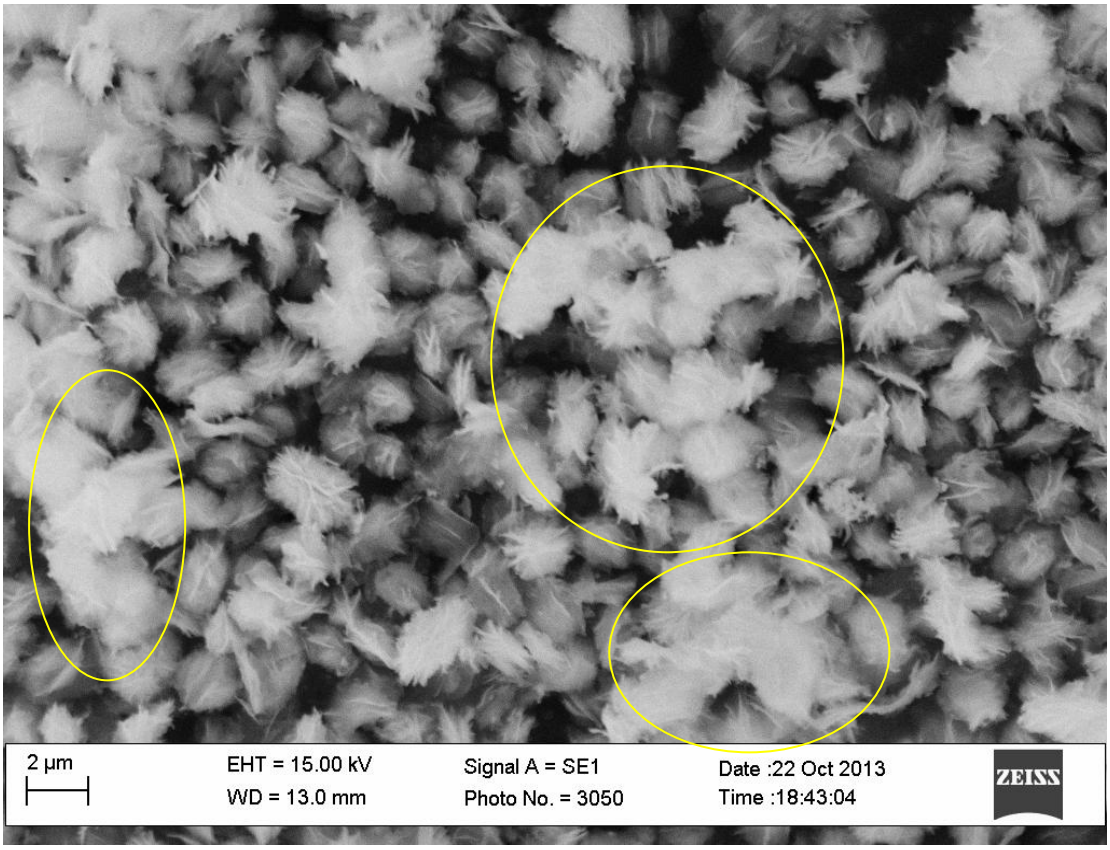

Figure 6. Formation of 3D flowerlike micro/nanocomposite ceria when the synthesis of ceria was carried out at 180 ℃ using a temperature-controlled oil bath and $CeCl_3 \cdot 7H_2O$ as the source of cerium. The circles represent the aggregates of 3D flowerlike ceria.

When Figure 6 was compared with the SEM image of 3D flowerlike ceria obtained by Zhong *et al*., the sizes and the distribution of 3D flowerlike ceria were different.[23] The size of individual ceria "flowers" in Figure 6 is about 2 µm whereas the ceria flowers synthesized by Zhong *et al*. were about 5 µm in diameter.[23] According to Zhong *et al*., further aggregation of 3D flowerlike ceria is prevented once the 3D flowerlike structure is formed because 3D flowerlike ceria is already present in an aggregated form.[23] However, some of the 3D flowerlike ceria appeared to clump together more than others in Figure 6. Thus, the aggregated 3D flowerlike ceria in Figure 6 was less evenly distributed and had fewer compact layers than the 3D flowerlike ceria that was synthesized by Zhong *et al*.[23] It is possible that the

aggregated 3D flowerlike ceria caused the dispersed 3D flowerlike ceria to clump together, which may have impeded the distribution of the dispersed 3D flowerlike ceria. Having an even distribution of 3D flowerlike micro- and nano-structure of ceria is important because it is required for microfiltration and because its aggregation may inhibit the adsorption of As(V) and Cr(VI), which could lower the efficiency of the 3D flowerlike ceria in water treatment.

3.1.2 ATR-IR

The ATR-IR spectra of TBAB, the ceria precursor, and the calcined ceria were obtained to study their chemical composition and to confirm that all the organic compounds were removed after calcination. As shown in Figure 7, the significant absorption bands for TBAB appeared at 1400 cm^{-1} (C-N stretch), 1500 cm^{-1} (C-H bend), and 2800-3000 cm^{-1} (C-H stretch).

The significant absorption bands for the ceria precursor appeared at 500-600 cm^{-1} (Ce-O stretch), 1000-1100 cm^{-1} (C-O stretch), 1300-1400 cm^{-1} (O-C-O symmetric stretch), 1400-1500 cm^{-1} (O-C-O asymmetric stretch), and 3100-3300 cm^{-1} (O-H stretch).[53] The absorption band for the Ce-O stretch appeared as a broad peak with the highest absorbance because the ceria precursor is mostly composed of cerium and oxygen. The vibrational frequency for the Ce-O stretch at 500-600 cm^{-1} agreed with the literature vibrational frequency at 551 cm^{-1}.[54] The O-C-O bonds in the ceria precursor are the alkoxide chains that link the cerium oxide molecules (Scheme 1). Two peaks were observed for the O-C-O band because the bond has both asymmetric stretching at a higher vibrational frequency and symmetric stretching at a lower vibrational frequency. In addition, the ceria precursor appeared to have either water or formic acid as a broad band for O-H stretching was observed at 3300-3400 cm^{-1}.

In the spectrum of the calcined ceria, the significant absorption bands that were observed appeared at 500-600 cm^{-1} (Ce-O stretch), 1300-1500 cm^{-1} (O-C-O asymmetric and symmetric stretches), and 3300-3400 cm^{-1} (O-H stretch). Similar to the ceria precursor, the calcined ceria was mostly composed of cerium and oxygen; thus, the absorption band for the Ce-O stretch was expected to have the highest absorbance. The absorption band for the O-C-O stretch still appeared after calcination at 450 ℃. Although all the alkoxide chains were not calcined, the absorption band of the O-C-O stretch for the calcined ceria had lower absorbance than that for the ceria precursor. As a result, the large quantities of the alkoxide chains were successfully removed in the calcined ceria. During calcination, not only most of the alkoxide chains, but also TBAB, which is an organic templating agent, was removed because the C-H stretch, the C-H bend, and the C-N stretch diminished after calcination. However, similar to the ceria precursor, the calcined ceria still contained water or formic acid as a broad band for O-H stretching was also observed at 3300-3400 cm^{-1}.

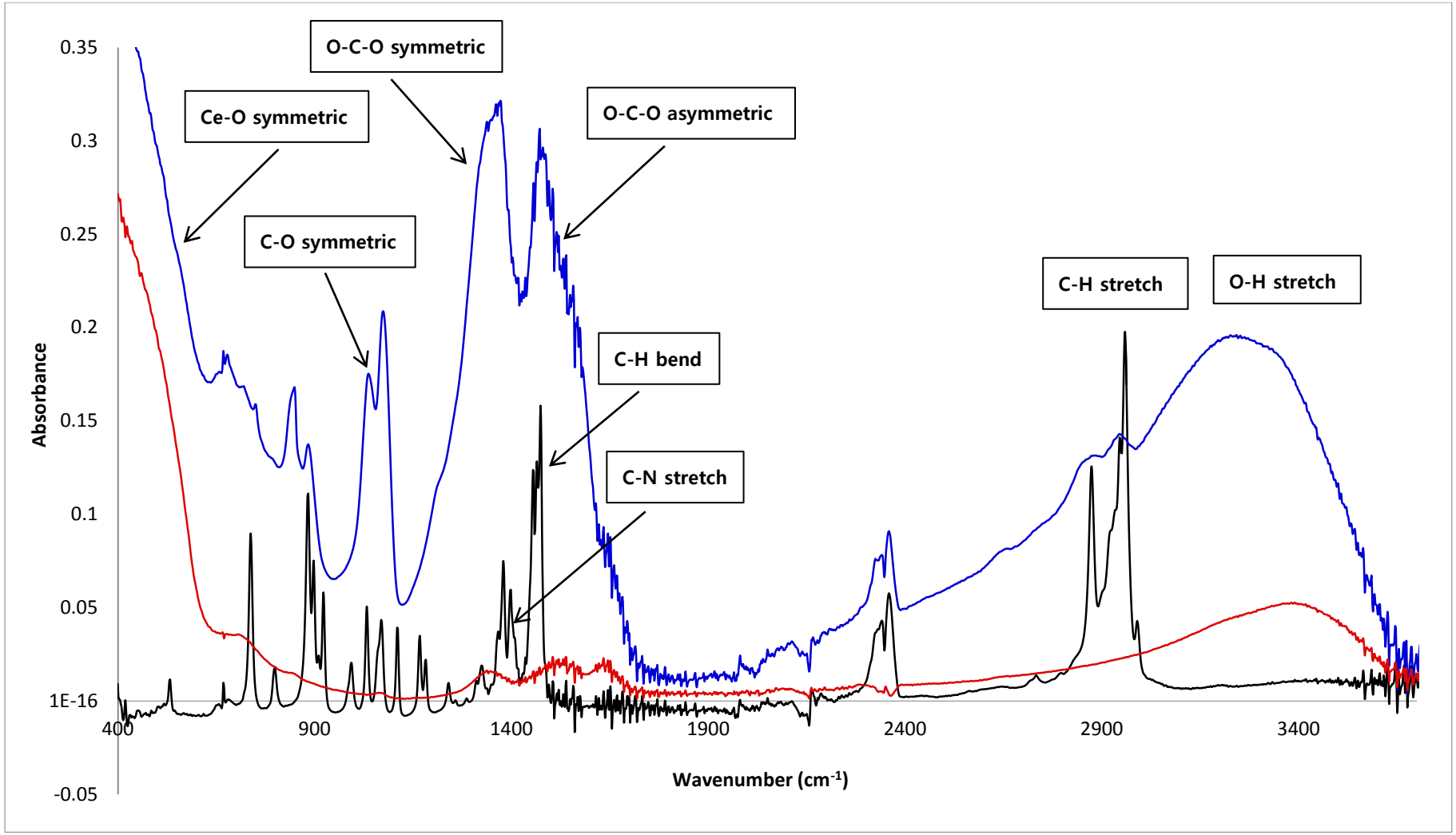

Figure 7. ATR-IR spectra of TBAB (black), ceria precursor (blue), and the calcined ceria (red).

3.1.3 Powder XRD

Powder XRD spectra were obtained for the ceria precursor (Figure 8) and the calcined ceria (Figure 9) to determine whether or not the 3D flowerlike ceria was in a highly crystalline phase after calcination.

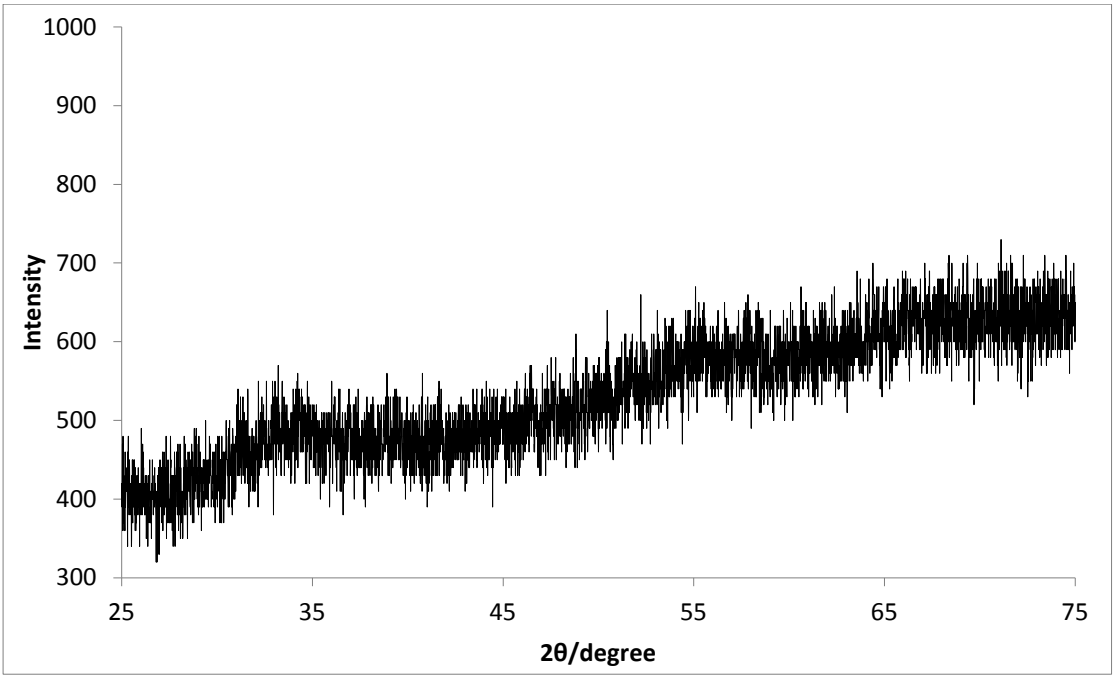

Figure 8. Powder XRD spectrum of the ceria precursor.

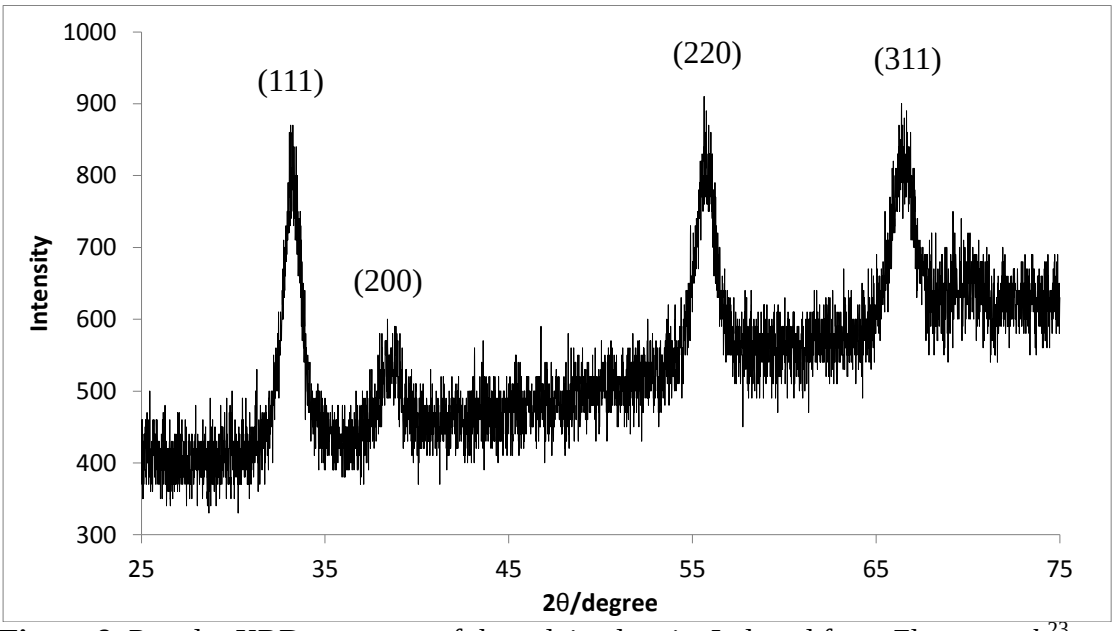

Figure 9. Powder XRD spectrum of the calcined ceria. Indexed from Zhong *et al*.[23]

As shown in Figure 8, there are no significant peaks in the powder XRD spectrum of the ceria precursor; this indicated that the ceria precursor was in an amorphous phase, in agreement with Zhong *et al*.[23] When the X-rays hit the ceria precursor, they were scattered in many directions; thus, only the ceria precursor was in non-crystalline phase because there was no constructive interferences.

However, four significant peaks appeared after calcination in Figure 9. When the X-rays hit the calcined ceria, peaks with high intensity appeared in the XRD spectrum because the X-rays hit the lattice planes of the calcined ceria and were preferentially scattered in certain directions.[55] Hence, the calcined ceria was in a crystalline phase, as evidenced by the sharp peaks with relatively higher intensities (Figure 9). It is important to have the calcined ceria in a crystalline phase because when the calcined ceria is in a highly crystalline phase, it has high surface area and a highly porous structure; both of these properties potentially increase the removal of As(V) and Cr(VI) by ceria. The four sharp peaks in the powder XRD spectrum of the calcined ceria agreed with the results from Shirke *et al*.[56] In order to study the structure of 3D flowerlike ceria further, the values of d-spacing were calculated using Equation 1 (Table 2). The d-spacings for our 3D flowerlike ceria match those reported by Shirke and his colleagues (Table 2).[56]

Table 2. Comparison of the experimental and the literature quantitative powder XRD data for the calcined ceria.

	λ of X-ray (Å)	2θ (degree)	θ (degree)	θ (radian)	sin θ	d-spacing (Å)
Experimental	1.79 (Cu)	33.0	16.5	0.288	0.284	3.15
		38.0	19.0	0.331	0.325	2.75
		55.5	27.8	0.484	0.465	1.92
		66.0	33.0	0.576	0.544	1.64
Shirke *et* a*l.*[56]	2.28 (Cr)	42.9	21.4	0.374	0.365	3.13
		50.2	25.1	0.438	0.424	2.70
		73.9	36.9	0.644	0.601	1.91
		89.0	44.5	0.776	0.701	1.63

3.2 Removal of As(V) and Cr(VI) from Water

Experiments were conducted to test the ability of the 3D flowerlike ceria to remove As(V) and Cr(VI) from water. Results from these experiments are shown in Figure 10.

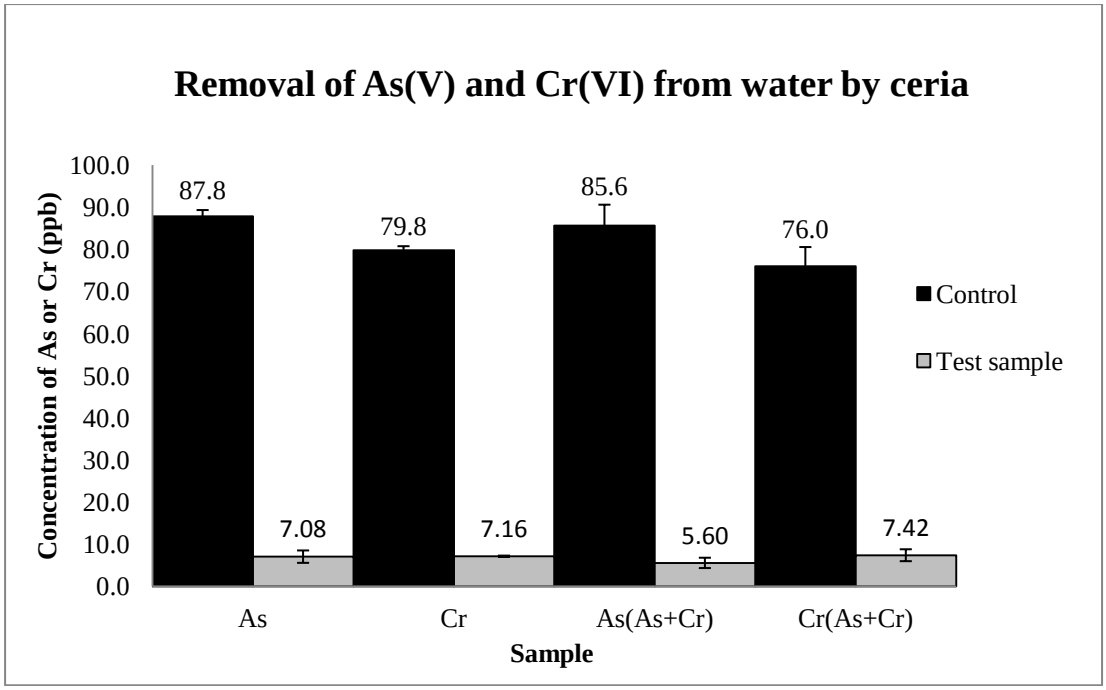

Figure 10. Removal of As(V) and Cr(VI) from water by ceria. Black bars represent controls without exposure to ceria, whereas grey bars represent test samples with exposure to ceria. (As + Cr) is a mixed solution of As(V) and Cr(VI). Numbers represent concentrations of corresponding samples listed. Error bars represent standard deviations for triplicate samples.

As shown in Figure 10, there was a significant decrease in the concentrations of As(V) and Cr(VI) after exposure to 3D flowerlike ceria. The final concentrations of As(V) and Cr(VI) were lower than the MCLs for As(V)[1] and Cr(VI)[3] in drinking water set by the U.S. EPA (Figure 10).[1,3] It is crucial to have lower concentrations of As(V) and Cr(VI) than their MCLs because the concentrations of As(V) and Cr(VI) that are higher than the MCLs will most likely cause serious health effects. The current drinking water standard for arsenic was lowered to be 10 ppb from 50 ppb in 1975 to reduce the public health risks from arsenic contamination in drinking water.[57] The percent removal of As(V) and Cr(VI) by the 3D flowerlike ceria were calculated and are summarized in Table 3.

Table 3. Percent removal of As(V) and Cr(VI) from water by 3D flowerlike ceria.

Sample	Removal by ceria (%)
As	92 ± 3
Cr	91 ± 2
As (As+Cr)	94 ± 8
Cr (As+Cr)	90 ± 8

In all test samples, the concentrations of As(V) and Cr(VI) were reduced by more than 90% using the 3D flowerlike ceria (Table 3). There were no significant differences among the removal percentages for the four samples within error. Therefore, there was no difference in removal in the single-contaminant solutions vs. the mixed solution; this revealed that the presence of both As(V) and Cr(V) ions did not affect the ability of the ceria to remove both ions. Also, since the removal percentages of the two mixed As(V) and Cr(V) samples were very close, the ceria did not preferentially remove one ion over the other ion.

3.3 Recovery and Recycling of 3D Flowerlike Ceria

After testing the removal of As(V) and Cr(VI) by the 3D flowerlike ceria, SEM images of the exposed (Figure 11) and NaOH-washed (Figure 12) ceria were obtained to determine if there were any morphological changes in the 3D flowerlike structure.

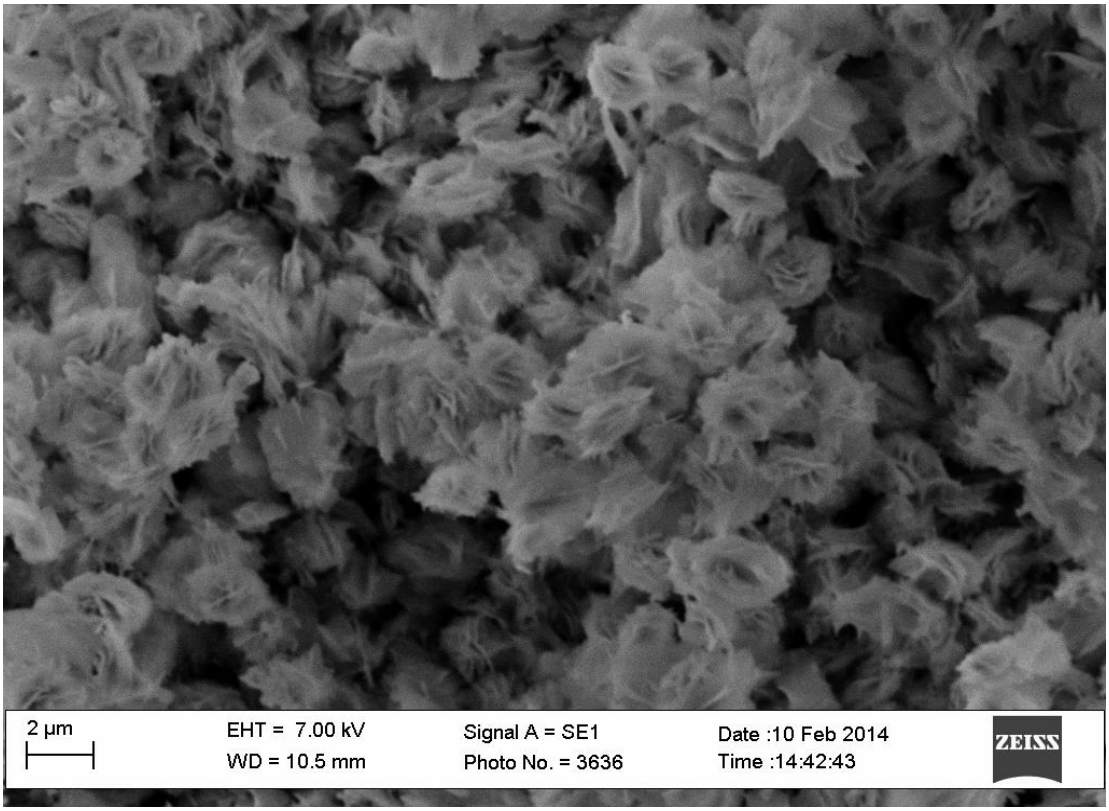

Figure 11. 3D flowerlike micro/nanocomposite ceria after exposure to As(V) and Cr(VI).

Figure 11 was compared with Figure 6 to determine if there were any morphological changes in the structure of the 3D flowerlike ceria after exposure to As(V) and Cr(VI). Based on this comparison, it is clear that the structure of the 3D flowerlike ceria was retained after it was exposed to the mixed As(V) and Cr(VI) solution. It is crucial to retain the 3D flowerlike micro/nanostructure because the 3D flowerlike micro/nanostructure allowed As(V) and Cr(VI) to sequester between the two stacked cerium-oxygen sheets and remove them from water.

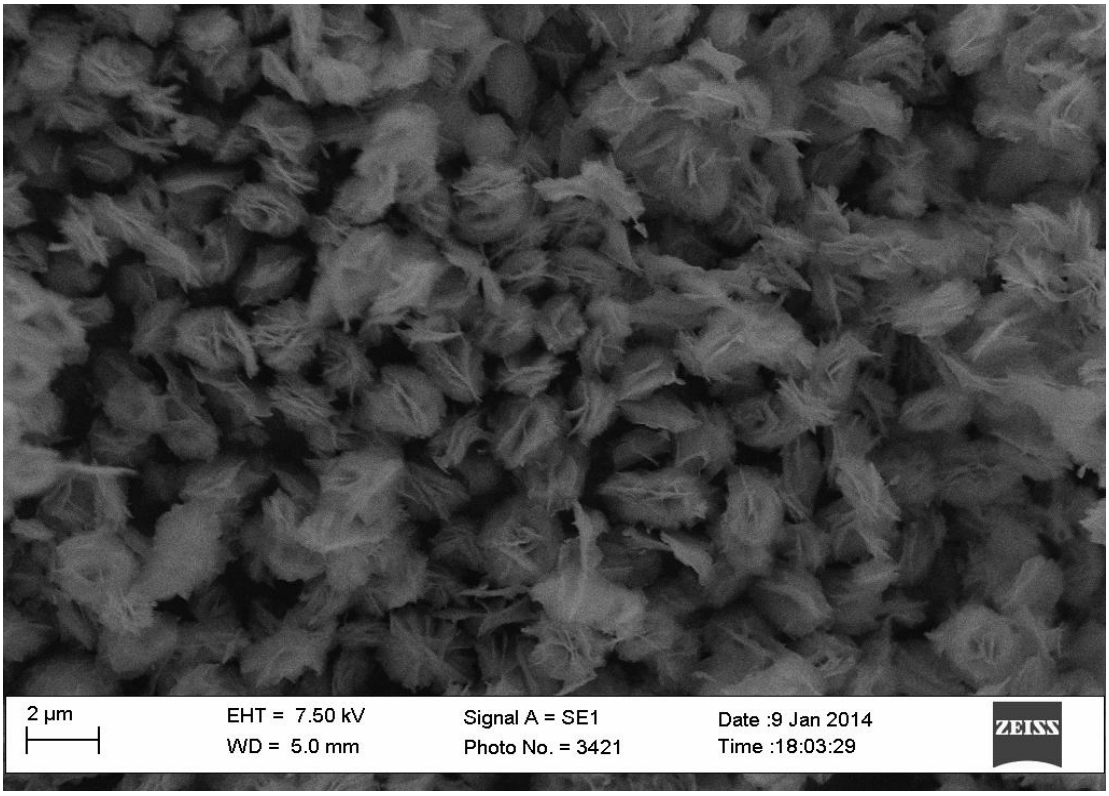

Figure 12. 3D flowerlike micro/nanocomposite ceria that was washed in NaOH solution after exposure to As(V) and Cr(VI).

After confirming that there was no change in morphology of the 3D flowerlike ceria after exposure to As(V) and Cr(VI), an SEM image of the ceria after regeneration (washing in NaOH) was obtained (Figure 12). Similar to the comparison between Figures 6 and 11, there was no change in morphology of the 3D flowerlike ceria upon washing with NaOH. The stability of the 3D flowerlike structure is important to be able to reuse the 3D flowerlike ceria after use and washing with NaOH solution. If there was any significant morphology change of the 3D flowerlike ceria after washing with NaOH, its properties would also change, and it could not be reused multiple times.

3.4 Testing the Dispersion of Laponite RD in the As(V) and Cr(VI) Solutions

When Laponite RD was added to the As(V) and Cr(VI) solutions and

centrifuged, it did not separate as a solid in the As(V) and Cr(VI) solutions; instead, it remained completely dispersed in the As(V) and Cr(VI) solutions. The dispersion of Laponite RD in the As(V) and Cr(VI) solutions is important because its dispersive property would facilitate to form the Laponite RD/3D flowerlike ceria filtration membrane.

3.5 Importance of Nanostructures

This experiment emphasizes that the cooperation of micro- and nano-structures of 3D flowerlike ceria is essential for water filtration applications. Several reports have emerged about various morphologies of ceria. For instance, Ho *et al*. have synthesized spherical ceria nanoparticles, microsized rod-shaped, and spindle-like ceria structures using a polyol method.[30] Ceria particles with these structures have been selected as catalysts for CO oxidation and have applications in solid electrolytes and electrochromic devices.[30] Li *et al*. have prepared mesoporous nanorod-like ceria by microwave-assisted hydrolysis of $Ce(NO_3)_3 \cdot 6H_2O$ in the presence of urea.[58] They reported that the mesoporous nanorod-like ceria has an application for efficient photocatalytic environmental purification because it exhibited highly efficient photothermocatalytic activity for the gas-phase mineralization of organic contaminants such as benzene.[58]

Sun *et al*. have fabricated nearly monodisperse flowerlike ceria microspheres that are hollow mesoporous materials with controlled morphologies and high hydrothermal stability.[31] The flowerlike ceria microsphere is an excellent candidate for gas transport due to its open 3D porous structure.[31] The monodisperse porous materials can be used as catalysis, energy storage, and conversation.[31] Similar to nearly monodisperse flowerlike ceria microspheres, Xiao *et al*. have synthesized

hierarchical ceria nanocrystal microspheres by a nonaqueous sol-gel method at 120 °C.[59] These microspheres appeared to be promising adsorbents for wastewater treatment because these can effectively remove Cr(VI) without pH preadjustment and rhodamine B from simulated wastewater.[59] Based on these studies of different morphologies of ceria nanomaterials, the nanostructure of ceria is a decisive factor for its applications.

3.6 An Emerging Ceria Nanostructure with Higher Removal Capacity for As(V) and Cr(VI): Ceria Hollow Nanospheres

Cao *et al*. extended the work of Zhong *et al*.[23] to investigate what morphology of ceria would give a better removal capacity for As(V) and Cr(VI).[60] Cao *et al*. have synthesized ceria hollow nanospheres by a template-free and microwave-assisted method.[60] The Brunauer-Emmett-Teller (BET) surface area and the maximum removal capacity of As(V) and Cr(V) for ceria hollow nanospheres were compared with those for 3D flowerlike ceria (Table 4).

Table 4. BET surface area and the maximum removal capacity of ceria hollow nanospheres and 3D flowerlike ceria.

Adsorbent sample	Brunauer-Emmett-Teller (BET) Surface area ($m^2 \cdot g^{-1}$)	Maximum removal capacity of As(V) ($mg \cdot g^{-1}$)	Maximum removal capacity of Cr(VI) ($mg \cdot g^{-1}$)
Ceria hollow spheres from Cao *et al*.[60]	72	22.4	15.4
3D flowerlike ceria from Zhong *et al*.[23]	34.1	14.4	5.9

As compared in Table 4, ceria hollow nanospheres have higher surface area and higher removal capacity for As(V) and Cr(VI) than 3D flowerlike ceria. In contrast to previously reported methods for other ceria nanostructures, neither an organic templating agent nor an organic solvent is needed to synthesize ceria hollow nanospheres.[60] In addition, microwave-assisted heating has advantages in low cost and short reaction time compared to the hydrothermal process.[60] Cao *et al*. also reported that microwave heating gives the homogeneous shapes and sizes of the nanoparticles due to uniform heating of the mixture.[60] For these reasons, they claimed that ceria hollow nanospheres are more advantageous than 3D flowerlike ceria to remove As(V) and Cr(VI) from water.

4. CONCLUSIONS

In summary, the 3D flowerlike ceria was successfully synthesized through a facile, ethylene glycol/TBAB mediated self-assembly process and was characterized using SEM, XRD, and ATR-IR. ICP-MS data revealed that the 3D flowerlike ceria sorbed As(V) and Cr(VI) in test solutions and reduced their aqueous concentrations by more than 90%. The 3D flowerlike micro/nanocomposite structure of ceria was retained both after exposure to As(V) and Cr(VI) and after washing with NaOH solution.

5. FUTURE WORK

5.1 Testing the Recycling and Reuse of 3D Flowerlike Ceria

One of the advantages of using 3D flowerlike ceria is that it can theoretically be reused multiple times.[23,60] Thus, it is important to test if the NaOH-washed 3D flowerlike ceria still has the same ability to reduce the concentrations of As(V) and

Cr(VI) in water. In order to test the reusability of the NaOH-washed 3D flowerlike ceria, it can be sequentially added to new As(V) and Cr(VI) solutions and centrifuged. If the final concentrations of As(V) and Cr(VI) are reduced by at least 90%, then the NaOH-washed 3D flowerlike ceria can be recycled and reused multiple times.

5.2 Selectivity of 3D Flowerlike Ceria for As(V) and Cr(VI)

In the current work, sodium arsenate dibasic heptahydrate and potassium dichromate were dissolved in deionized water to prepare As(V) and Cr(VI) solutions for water treatment. In the future, it would be ideal to test the ability of 3D flowerlike ceria to remove As(V) and Cr(VI) in actual contaminated drinking water samples. There may be other potential contaminants such as magnesium and calcium present in contaminated drinking water. It would be interesting to test if the 3D flowerlike ceria can selectively remove As(V) and Cr(V) from contaminated drinking water in the presence of other metals and ions.

5.3 Laponite RD/3D Flowerlike Ceria Filtration Membrane

Since Laponite RD remained dispersed in the As(V) and Cr(VI) solutions, the 3D flowerlike ceria can be incorporated within Laponite RD to create water filtration membranes. The proposed scheme of Laponite RD/3D flowerlike ceria filtration membrane is shown in Figure 13.

After confirming the aqueous dispersion of Laponite RD in the As(V) and Cr(VI) solutions, the simultaneous addition of Laponite RD and the 3D flowerlike ceria to the As(V) and Cr(VI) solutions may help to disperse the 3D flowerlike ceria aggregates. Increasing dispersion of 3D flowerlike ceria may increase its ability to remove As(V) and Cr(VI) because more surface area of the 3D flowerlike ceria will

be exposed to adsorb more As(V) and Cr(VI).

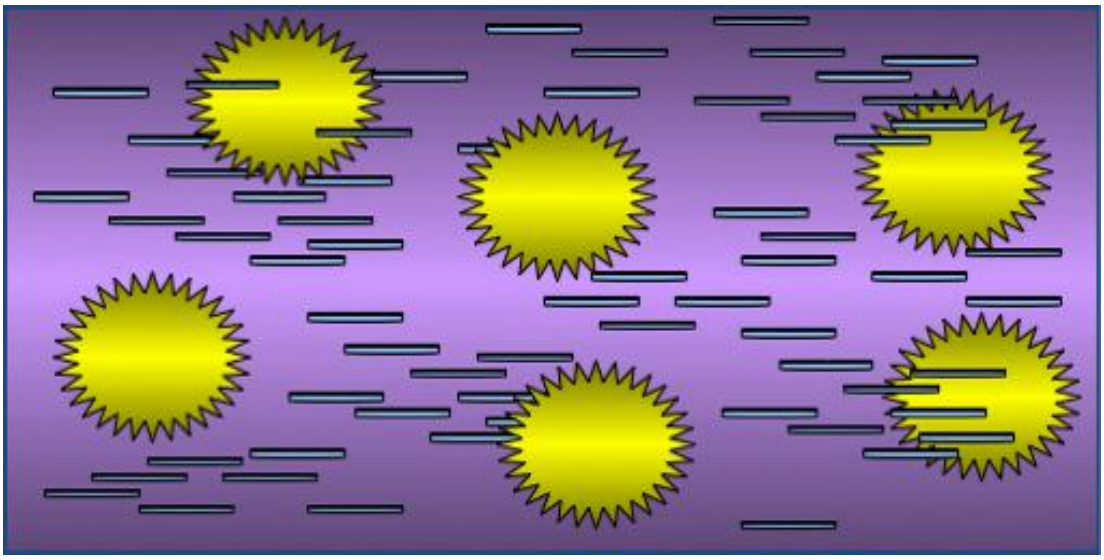

Figure 13. Proposed scheme of Laponite RD/3D flowerlike ceria filtration membrane. Yellow flowers and blue disks represent 3D flowerlike ceria and Laponite RD, respectively.

In order to create the Laponite RD/3D flowerlike ceria filtration membrane, Laponite RD and 3D flowerlike ceria can be added to the As(V) and Cr(VI) solutions simultaneously and centrifuged to allow Laponite RD to separate with the 3D flowerlike ceria. The precipitate can be collected and air-dried. The air-dried precipitate can be casted on filter paper,[36] and the morphology of the Laponite RD/3D flowerlike ceria filtration membrane can be studied using SEM. The final concentrations of As(V) and Cr(VI) after the addition of Laponite RD and 3D flowerlike ceria can be measured by using ICP-MS. The percent removal of the Laponite RD/3D flowerlike ceria filtration membrane can be compared with the percent removal of As(V) and Cr(VI) after exposure to 3D flowerlike ceria.

References

1. Arsenic in drinking water. http://water.epa.gov/lawsregs/rulesregs/sdwa/arsenic/index.cfm (accessed on June 10, 2014).
2. Agency for Toxic Substances and Disease Registry, U.S. Department of Health and Human Services. *Toxicological profile for chromium*. September 2000.
3. Chromium in drinking water. http://water.epa.gov/drink/info/chromium/#one (accessed on June 10, 2014).
4. Smith, A. H.; Lingas, E. O.; Rahman, M. Contamination of drinking-water by arsenic in Bangladesh: a public health emergency. *B. World Health Organ.* **2000**, *78*, 1093-1103.
5. Layton, L. Probable carcinogen hexavalent chromium found in drinking water of 31 U.S. cities. The Washington Post [Online], December 19, 2010. 1-2. http://www.washingtonpost.com/wpdyn/content/article/2010/12/18/AR2010121802810.html (accessed on May 4, 2014).
6. Savage, N.; Diallo, M. Nanomaterials and water purification: Opportunities and challenges. *J. Nanopart. Res.* **2005**, *7*, 331-342.
7. Obare, S. O.; Meyer, G. J. Nanostructured materials for environmental remediation of organic contaminants in water. *J. Environ. Sci. Heal. A.* **2004**, *39*, 2549–2582.
8. Adesina, A. A. Industrial exploitation of photocatalysis progress, perspectives and prospects. *Catal. Surv. Asia* **2004**, *8*, 265–273.
9. Schrick, B.; Blough, J. L.; Jones, A. D.; Mallouk, T. E. Hydrodechlorination of trichloroethylene to hydrocarbons using bimetallic nickel-iron nanoparticles. *Chem. Mater.* **2002**, *14*, 5140–5147.
10. Zhang, W. X. Nanoscale iron particles for environmental remediation. *J.*

Nanopart. Res. **2003**, *5*, 323–332.

11. Nurmi, J. T.; Tratnyek, P. G.; Sarathy, V.; Baer, D. R.; Amonette, J. E.; Pecher, K.; Wang, C.; Lineham, J. C.; Matson, D. W.; Penn, R. L.; Driessen, W. D. Characterization and properties of metallic iron nanoparticles: Spectroscopy, electrochemistry, and kinetics. *Environ. Sci. Technol.* **2005**, *39*, 1221–1230.
12. Vander Bruggen, B.; Vandecasteele, C. Removal of pollutants from surface water and groundwater by nanofiltration overview of possible applications in the drinking water industry. *Environ. Pollut*. **2003**, *122*, 435–445.
13. Favre-Reguillon, A.; Lebuzit, G.; Fooz, J.; Guy, A. Selective concentration of uranium from seawater by nanofiltration. *Ind. Eng. Chem. Res*. **2003**, *42*, 5900–5904.
14. Peltier, S.; Cotte, E.; Gatel, D.; Herremans, L.; Cavard, J. Nanofiltration improvements of water quality in a large distribution system. *Water Sci. Technol*. **2003**, *3*, 193–200.
15. Ottaviani, M. F.; Favuzza, P.; Bigazzi, M.; Turro, N. J.; Jockusch, S.; Tomalia, D. A. A TEM and EPR investigation of the competitive binding of uranyl ions to starburst dendrimers and liposomes: Potential use of dendrimers as uranyl ion sponges. *Langmuir* **2000**, *16*, 7368–7372.
16. Birnbaum, E. R.; Rau, K.C.; Sauer, N. N. Selective anion binding from water using soluble polymers. *Sep. Sci. Technol.* **2003**, *38*, 389–404.
17. Diallo, M. S.; Christie, S.; Swaminathan, P.; Balogh, L.; Shi, X.; Um, W.; Papelis, C.; Goddard III, W. A.; Johnson Jr., J. H. Dendritic chelating agents 1. Cu(II) binding to ethylene diamine core poly(amidoamine) dendrimers in aqueous solutions. *Langmuir* **2004**, 20, 2640–2651.
18. Li, Y. H.; Ding, J.; Luan, Z. K.; Di, Z. C.; Zhu, Y. F.; Xu C. L.; Wu, D. H.; Wei,

B. Q. Competitive adsorption of Pb^{2+}, Cu^{2+}, and Cd^{2+} ions from aqueous solutions by multiwalled carbon nanotubes. *Carbon* **2003**, *41*, 2787–2792.

19. Moreno, N.; Querol, X.; Ayora, C. Utilization of zeolites synthesized from coal fly ash for the purification of acid mines water. *Environ. Sci. Technol.* **2001**, *35*, 3526–3534.
20. Peng, X.; Luan, Z.; Ding, J.; Di, Z.; Li, Y.; Tian, B. Ceria nanoparticles supported nanotubes for the removal of arsenate from water. *Mater. Lett.* **2005**, *59*, 399–403.
21. Deliyanni, E. A.; Bakoyannakis, D. N.; Zouboulis, A. I.; Matis, K. A. Sorption of As(V) ions by akaganeite-type nanocrystals. *Chemosphere* **2003**, *50*, 155–163.
22. Lazaridis, N. K.; Bakoyannakis, D. N.; Deliyanni, E. A. Chromium(VI) sorptive removal from aqueous solutions by nanocrystalline akaganeite. *Chemosphere* **2005**, *58*, 65–73.
23. Zhong, L. S.; Hu, J. S.; Cao, A. M.; Liu, Q.; Song, W. G.; Wan L. J. 3D Flowerlike ceria micro/nanocomposite structure and its application for water treatment and CO removal. *Chem. Mater.* **2007**, *19*, 1648-1655.
24. Terribile, D.; Trovarelli, A.; Llorca, J.; de Leitenburg, C.; Dolcetti, G. The synthesis and characterization of mesoporous high-surface-area ceria prepared using hybrid organic inorganic route. *J. Catal.* **1998**, *178*, 299-308.
25. Trovarelli, A.; de Leitenburg, C.; Boaro, M.; Dolcetti, G. The utilization of ceria in industrial catalysis. *Catal. Today* **1999**, *50*, 353-367.
26. Flytzani-Stephanopoulos, M.; Sakbodin, M.; Wang, Z. Regenerative adsorption and removal of H_2S from hot fuel gas streams by rare earth oxides. *Science*, **2006**, *312*, 1508-1510.
27. Peng, X. J.; Luan, Z. K.; Ding, J.; Di, Z. C.; Li, Y. H.; Tian, B. H. Ceria nanoparticles supported on carbon nanotubes for the removal of arsenate from

water. *Mater. Lett*. **2005**, *59*, 399-403.

28. Di, Z. C.; Ding, J.; Peng X. J.; Li, Y. H.; Luan, Z. K.; Liang J. Chromium adsorption by aligned carbon nanotubes supported ceria nanoparticles. *Chemosphere* **2006**, *62*, 861-865.
29. Masciangioli, T.; Zhang, W. X. Environmental technologies at the nanoscale. *Environ. Sci. Technol.* **2003**, *37*, 102A-108A.
30. Ho, C.; Yu, J. C.; Kwong, T.; Mak, A. C.; Lai, S. Morphology-controllable synthesis of mesoporous CeO_2 nano- and microstructures. *Chem. Mater*. **2005**, *17*, 4514-4522.
31. Sun, C.; Sun, J.; Xiao, G.; Zhang, H.; Qiu, X.; Li, H.; Chen, L. Mesoscale organization of nearly monodisperse flowerlike ceria microspheres. *J. Phys. Chem. B* **2006**, *110*, 13445-13452.
32. Liu, J.; Liu, G.; Zhang, M.; Sun, P.; Zhao, H. Synthesis and self-assembly of amphiphilic Janus Laponite disks. *Macromolecules* **2013**, *46*, 5974–5984.
33. Ruzicka, B.; Zulian, L.; Ruocco, G. More on the phase diagram of Laponite. *Langmuir* **2006**, *22*, 1106−1111.
34. Mourchid, A.; Delville, A.; Lambard, J.; Lecolier, E.; Levitz, P. Phase diagram of colloidal dispersions of anisotropic charged particles: equilibrium properties, structure, and rheology of Laponite suspensions. *Langmuir* **1995**, *11*, 1942−1950.
35. Walt, D. R. Fiber optic imaging sensors. *Acc. Chem. Res.* **1998**, *31*, 267-278.
36. Kehlbeck, J. D.; Hagerman, M. E.; Cohen, B. D.; Eliseo, J.; Fox, M.; Hoek, W.; Karlin, D.; Leibner, E.; Nagle, E.; Nolan, M.; Schaefer, I.; Toney, A.; Topka, M.; Uluski, R.; Wood, C. Directed self-assembly in Laponite/CdSe/Polyaniline nanocomposites. *Langmuir* **2008**, *24*, 9727-9738.
37. Kim, J.; Lee, W.; Song, M.; Joo, J.; Campos L. C. Photocatalytic oxidation of TCE

in water using nano-ZnO/Laponite composite. Poster Presented at IWA World Water Congress, Korea, 2012.

38. Robinson, J. W.; Skelly Frame, E. M.; Frame II, G. M. *Undergraduate Instrumental Analysis*, 6th ed.; Marcel Dekker: New York, 2005.
39. UCDavisChemWiki. UV/Vis and IR spectroscopy. http://chemwiki.ucdavis.edu/Analytical_Chemistry/Analytical_Chemistry_2.0/10_Spectroscopic_Methods/10C_UV%2F%2FVis_and_IR_Spectroscopy (accessed November 12, 2013).
40. Harris, D. C. *Quantitative Chemical Analysis*, 8th ed.; W. H. Freeman and Company: New York, 2010.
41. Wang, Q.; Padua, V. *Nanotechnology Research Methods for Foods and Bioproducts*, 1st ed.; John Wiley & Sons: Ames, 2012.
42. Swapp, S. Geochemical instrumentation and analysis: scanning electron microscopy. serc.carleton.edu/research_education/geochemsheets/techniques/SEM.html (accessed November 10, 2013).
43. Wittke, J. H. http://www4.nau.edu/microanalysis/Microprobe-SEM/Instrumentation.html (accessed February 8, 2013).
44. Scanning Electron Microscope A To Z: Basic Knowledge for Using the SEM. www.teksercorp.com/docs/jeol/sem/SEM_A_To_Z_light.pdf (accessed on February, 8 2014).
45. Carroll, M. Union College Chemical Instrumentation Class Notes. November 6, 2013.
46. Chemviews. 100th anniversary of the discovery of X-ray diffraction. http://www.chemistryviews.org/details/ezine/2064331/100th_Anniversary_of_the_Discovery_of_X-ray_Diffraction.html (accessed November 12, 2013).
47. Hollocher, K. ICP-MS analytical facility. http://minerva.union.edu/hollochk/icp-

ms/index.htm (accessed November 12, 2013).

48. Thomas, R. A. *Practical Guide to ICP-MS*. New York: Dekker, 2003.
49. Carroll, M. Union College Chemical Instrumentation Class Notes. October 25, 2013.
50. Labunlimited. Chromatography ICP-MS supplies. http://www.labunlimited.com/Online-Shop/Chromatography/ICP-MS-Supplies/Description (accessed November 12, 2013).
51. Skoog, D. A.; Holler, F. J.; Crouch, S. R. *Principles of Instrumental Analysis*, 6th ed.; Belmont: Brooks/Cole, 2007.
52. Kim, T.; MacManus-Spencer, L.; Hagerman, M. E. 3D Flowerlike ceria micro/nanocomposite structure and Laponite/ceria membranes for water treatment. *Presidential Green Grant Proposal* **2013**, 1-3.
53. Patil, H. M.; Sawant, D. K.; Bhavsar, D. S.; Patil, J. H.; Girase, K. D. Crystallographic and FT-IR characteristics of gel brown cerium tartrate crystals. *Arch. Phys. Res.* **2011**, *2*, 239-245.
54. Chelliah, M.; Rayappan, J. B. B.; Kirshnan, U. M. Synthesis and characterization of cerium oxide nanoparticles by hydroxide mediated approach. *J. Appl. Sci.* **2012**, *12*, 1734-1737.
55. Cullity, B. D.; Elements of X-ray diffraction. *Amer. J. Physics*, **1957**, *25*, 101-102.
56. Shirke, B. S.; Patil, A. A.; Hankare, P. P.; Garadkar, K. M. Synthesis of cerium oxide nanoparticles by microwave technique using propylene glycol as a stabilizing agent. *J. Mater. Sci: Mater. Electron* **2011**, *22*, 200-203.
57. Fact sheet: drinking water standard for arsenic. http://water.epa.gov/lawsregs/rulesregs/sdwa/arsenic/regulations_factsheet.cfm (accessed May 22, 2014).
58. Li, Y.; Sun, Q.; Kong, M.; Shi, W.; Huang, J.; Tang, J.; Zhao, X. Coupling oxygen

ion conduction to photocatalysis in mesoporous nanorod-like ceria significantly improves photocatalytic efficiency. *J. Phys. Chem. C* **2011**, *115*, 14050-14057.

59. Xiao, H.; Ai, Z.; Zhang, L. Nonaqueous sol-gel synthesized hierarchical CeO_2 nanocrystal microspheres as novel adsorbents for wastewater treatment. *J. Phys. Chem. C* **2009**, *113*, 16625-16630.
60. Cao, C.-Y.; Cui, Z.-M.; Chen, C.-Q.; Song, W.-G.; Cai, W. Ceria hollow nanospheres produced by a template-free microwave-assisted hydrothermal method for heavy metal ion removal and catalysis. *J. Phys. Chem. C* **2010**, *114*, 9865–9870.